Supporting Information

Green Synthesis Strategy for Lithium/Sodium-Ion Batteries Anode: Morphology and Structure-Engineered in Biochar to Boost the Comprehensive Electrochemical Performance

Likai Zhu[1], *Lijuan Men*[1], *Jiaying Chen*[1], *Bi Luo*[1], *Fanghua Xie*[1], *Wenli Zhang*[2], *Jiafeng Zhang*[3], *Yefeng Zhou*(✉)[1]

[1] National & Local United Engineering Research Centre for Chemical Process Simulation and Intensification, Chemical Process Simulation and Optimization Engineering Research Center of Ministry of Education, Xiangtan University, Xiangtan 411100, China

[2] Guangdong Provincial Key Laboratory of Plant Resources Biorefinery, School of Chemical Engineering and Light Industry, Guangdong University of Technology (GDUT), 100 Waihuan Xi Road, Panyu District, Guangzhou 510006, China

[3] National Engineering Laboratory for High-Efficiency Recovery of Refractory Nonferrous Metals, School of Metallurgy and Environment, Central South University, Changsha 410083, Hunan, China

*Corresponding author; E-mail address: zhouyf@xtu.edu.cn (Y. Zhou)

1. Experimental

1.1. Chemicals and Materials

In this study, camellia oleifera shells were mainly selected as the carbon-based precursors, and their chemical compositions are given in Table S1. In all experiments, an ultrapure purification system (YL-100, Shenzhen Yiliyuan Water Treatment Equipment Company Limited, Shenzhen, China) was used to produce 18.25 MΩ cm^{-1} of water.

Table S1. Chemical composition of the Camellia oleifera shells.

Sample	Elemental analysis (wt %)				
	C	O	H	S	N
Camellia oleifera shells	48.07	41.44	5.53	0.74	0.32

1.2. Preparation of CHCs-T

The camellia oleifera shells were obtained from Hunan, China. First, the camellia oleifera shells were washed and dried, and then pulverized in a small solid grinder. The resulting material was sieved through a 60-100 mesh sieve to obtain oil tea shell powder with an average particle size of 0.15-0.25 mm. Then, the camellia oleifera shells powder was mixed with ultrapure water at a mass ratio of 1:20, stirred for 30 min, and then treated with ultrasonic waves for 30 min to form a homogeneous biomass dispersion. The dispersion was transferred to a PTFE container and subjected to a first hydrothermal treatment in an oven at 220°C for 24 hours, after cooling, the mixture was filtered and ground to obtain unformed hydrothermal carbon powder. The unformed hydrothermal carbon powder was then placed in a crucible and transferred to a tube furnace under inert atmosphere. The samples were heated to temperatures of 500, 700, 900, and 1100°C under N_2 at a rate of 5°C/min and carbonized at each temperature for 30 min. After carbonization, the samples were cooled to room temperature and milled to obtain formed hard carbon powder. Finally, the hard carbon powder was mixed with ultrapure water at a mass ratio of 1:100 to again form a homogeneous biochar dispersion. The dispersion was transferred to a PTFE container and subjected to a

second hydrothermal treatment in an oven at 180°C for 24 hours, resulting in a quasi-spherical hard carbon granular material. Samples treated at different carbonization temperatures are designated as CHCs-500, CHCs-700, CHCs-900, and CHCs-1100, respectively. For the purpose of comparative analysis with CHCs-T materials, a hard carbon material was synthesized through direct carbonization at 900°C and designated as HC-900 (Figure S1).

1.3 Material Characterization

The crystal structure, degree of crystallinity, and phase composition of the materials were analyzed by X-ray diffraction (XRD, Rigaku SmartLab SE, Japan). Characterization of material structure by Raman spectroscopy (Raman, Horiba LabRAM HR Evolution, Japan). Chemical bonding or functional group information on the materials surface were obtained by Fourier transform infrared spectroscopy (FTIR, Nicolet 6700, Thermo Fisher Scientific, USA). Elemental analysis (EA, Elementar Vario EL III, Germany) and X-ray photoelectron spectroscopy (XPS, Thermo Scientific KAlpha, USA) were used to analyze the elemental composition, content, and elemental valence of the material surface. Specific surface area and pore volume distribution of the materials were analyzed by Brunel-Emmett-Teller analysis (BET, Micromeritics ASAP 2460, USA). The microstructure and morphology of the materials were analyzed by scanning electron microscopy (SEM, ZEISS Sigma 300, Germany) and high-resolution transmission electron microscopy (HRTEM, FEI Tecnai F20, USA).

1.4 Electrochemical Characterization

CHCs-T was used as the active materials. The active materials, acetylene black and polyvinylidene fluoride (PVDF) were mixed into a slurry in the ratio of 7:2:1 by mass and coated on the copper foil and dried at 110℃ for 12h. After cooling at room temperature, the copper foil was cut into circular electrode slices with a diameter of 14 mm using a slicing machine, and then the mass of the active substances was determined by weighing each electrode slice, which had 0.5 mg of active substance per electrode sheet with a face loading of 0.003248 mg mm^{-2}. The assembly of the lithium-ion batteries and sodium-ion batteries were carried out in a glove box in an Ar and

anhydrous atmosphere. For lithium-ion batteries, the cathode was lithium flakes, the electrolyte was $LiPF_6$ solution (1.0 m) dissolved in a solvent mixture consisting of dimethyl carbonate: ethyl carbonate: vinyl carbonate (DC/EC/VC=*v*/*v*/*v*=1:1:1), and the diaphragm was Celgard 2400. For sodium-ion batteries, the cathode was sodium flakes, the electrolyte was $NaPF_6$ solution (1.0 m) dissolved in a solvent mixture consisting of ethylene carbonate/propylene carbonate (EC/PC=*v*/*v*=1:1), and the diaphragm was GF/C Glass Fiber. In addition, the battery consumables (e.g., collectors, cases, etc.) used in this paper during the electrochemical testing experiments are commercially available materials (www. Shiyanjia.com) to ensure consistent quality specifications. The charging and discharging performances of the batteries were tested on the NEWWARE Battery Test System (CT-3008, China). Cyclic voltammetry (CV) and electrochemical impedance spectroscopy (EIS) were tested on the DH7000C electrochemical system (Jiangsu Donghua Analytical Instrument Co., Ltd.).

2. The relevant equations for electrochemical calculations

2.1 Calculating the Li^+/Na^+ diffusion coefficients based on EIS data

EIS is composed by two sections: (1) a semicircle at middle-high frequency region consists of contact resistance and charge transfer resistance; (2) a straight line at low frequency region belongs to the Warburg impedance.

$$\omega = 2\pi f \quad (S1)$$

$$Z'' = R + \sigma\omega^{-1/2} \quad (S2)$$

$$D = 0.5R^2T^2/S^2n^4F^4C^2\sigma^2 \quad (S3)$$

According to **Equation S1-S2**, the corresponding slope of Z'' *vs.* $\omega^{-1/2}$ is the Warburg diffusion parameter (σ). For **Equation S3**, R is the gas constant (8.314 J mol^{-1} K^{-1}), T is Kelvin temperature (293.15 K), S is the surface area of CHCs-T, T=500, 700,900 and 1100℃ (1.54 cm^2), n is the electronic transfer number, F is the Faraday constant (96485 C mol^{-1}) and C is the concentration of Li^+/Na^+ in the electrolyte.

2.2 Calculating the b value and capacitive contribution ratio

The parameter of ***b*** could be calculated as the slope value of the fitting linear of

log(i) vs. log(v).

$$i = av^b \quad (S4)$$

$$\log i = \log a + b\log v \quad (S5)$$

The response current (i) could be divided into two components by introducing new parameters of k_1 and k_2.

$$i = k_1 v + k_2 v^{1/2} \quad (S6)$$

$\boldsymbol{k_1 v}$ originates from the capacitive contribution, $\boldsymbol{k_2 v^{1/2}}$ originates from the diffusion-limited Faradaic processes. $\boldsymbol{k_1}$ value could be acquired through the linear relationship between $\boldsymbol{i/v^{1/2}}$ and $\boldsymbol{v^{1/2}}$.

3. Economic analysis

3.1 Material cost

This raw material cost statistics only include the cost of materials consumed in the one-time preparation process. Raw material prices refer to the international price on 2024.11.25.

Table S2 The prices and quantities of materials at all stages

Stage	Material	Unit Price	Quantity	Cost ($)
Pretreatment of Biomass	Camellia Oleifera Shell	0.042 $ Kg^{-1}	12 g	0.0005
	H_2O	0.071 $ Kg^{-1}	5 L	0.3550
First Hydrothermal Treatment	H_2O	0.071 $ Kg^{-1}	0.24 L	0.0170
Carbonization	N_2 (500℃)	0.063 $ Kg^{-1}	32 L	0.0025
	N_2 (700℃)	0.063 $ Kg^{-1}	40 L	0.0032
	N_2 (900℃)	0.063 $ Kg^{-1}	48 L	0.0038
	N_2 (1100℃)	0.063 $ Kg^{-1}	56 L	0.0044
Second Hydrothermal Treatment	H_2O	0.071 $ Kg^{-1}	0.15 L	0.0107
Washing	H_2O	0.071 $ Kg^{-1}	5 L	0.3550

3.2 Evaluation of energy consumption

This section evaluates the economics of the hydrothermal-carbonization-hydrothermal process in this study using power consumption(w) taking into account energy consumption.

$w = p * t$

In the first hydrothermal treatment (FHT), direct current was applied to prepare the unshaped hydrothermal carbon powder (experimental conditions: p =2.0 Kw, and heating time = 24 h, T=220°C). w_1 was then calculated:

$w_1 = p * t = w_{FHT} = 2 * 24 = 48\ KW\ h$

Hard carbon can be achieved through one carbonization process(experimental conditions: p =1.2 Kw, and heating time = 3.5 h). w_2 was then calculated:

$$w_2 = p * t = w_{SHT} = 1.2 * 3.5 = 4.2\ KW\ h$$

In the second hydrothermal treatment (SHT), direct current was applied to prepare the quasi-spherical hard carbon (experimental conditions: p =2.0 Kw, and heating time = 24 h, T=220°C). Since the temperatures of the two hydrothermal treatments were different, we further assessed the energy consumption of the second hydrothermal treatment to be 82% of the first hydrothermal treatment. w_3 was then calculated:

$w_3 = p * t = w_{SHT} = w_2 * 0.82 = 48 * 0.82 = 39.3\ KW\ h$

w_{Total} was then calculated:

$$w_{Total} = w_1 + w_2 + w_3 = 48 + 3.2 + 39.3 = 91.5\ KW\ h$$

Accordingly, the Supporting Information indicates that the power consumption of the quasi-spherical hard carbon preparation process is 91.5 KW h, with a unit electricity price of 0.069 $/(kW h), resulting in a required electricity price (c) of $6.31.

3.3 Comprehensive economic calculations

According to **Table S2** and **Equation S7-S11**, we calculated the cost of a single preparation of quasi-spherical carbon to be $6.31. It should be noted, however, that this economic evaluation represents only the cost of laboratory preparation, and that we can guarantee that we can scale up quasi-spherical carbon preparations by a factor of 5 while consuming the same preparation cost.

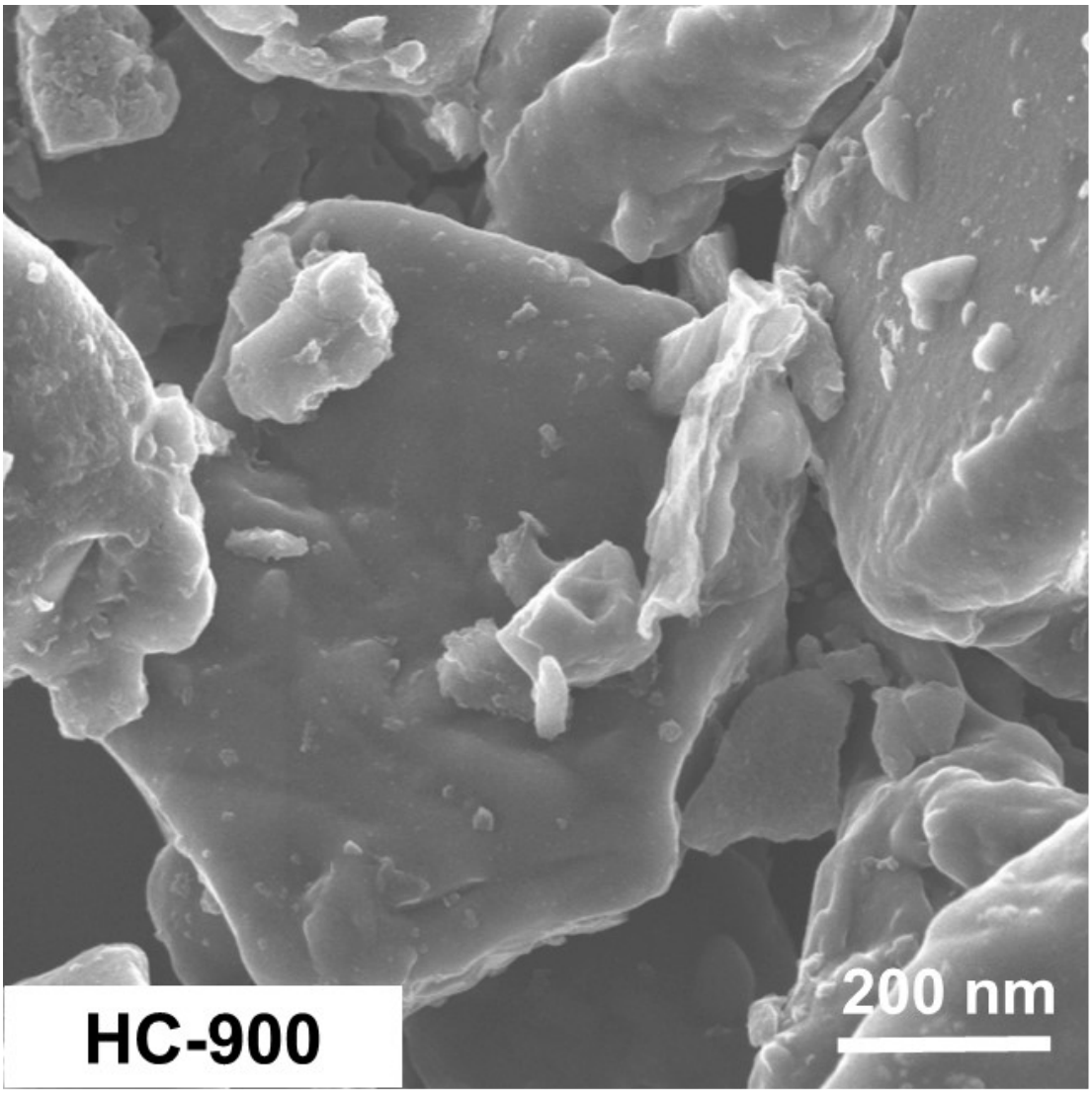

Fig. S1. SEM images of HC-900

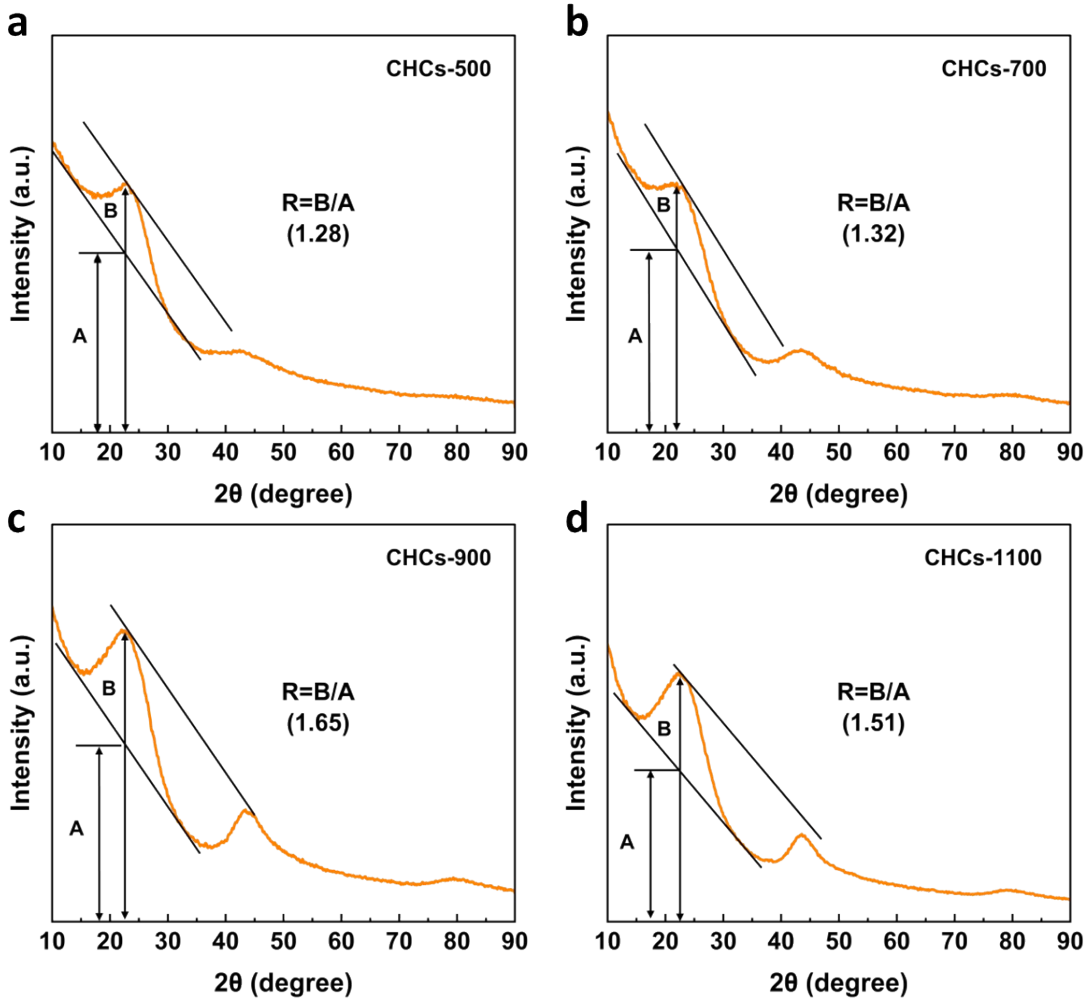

Fig. S2. Schematic of empirical R-value calculation for CHCs-T materials

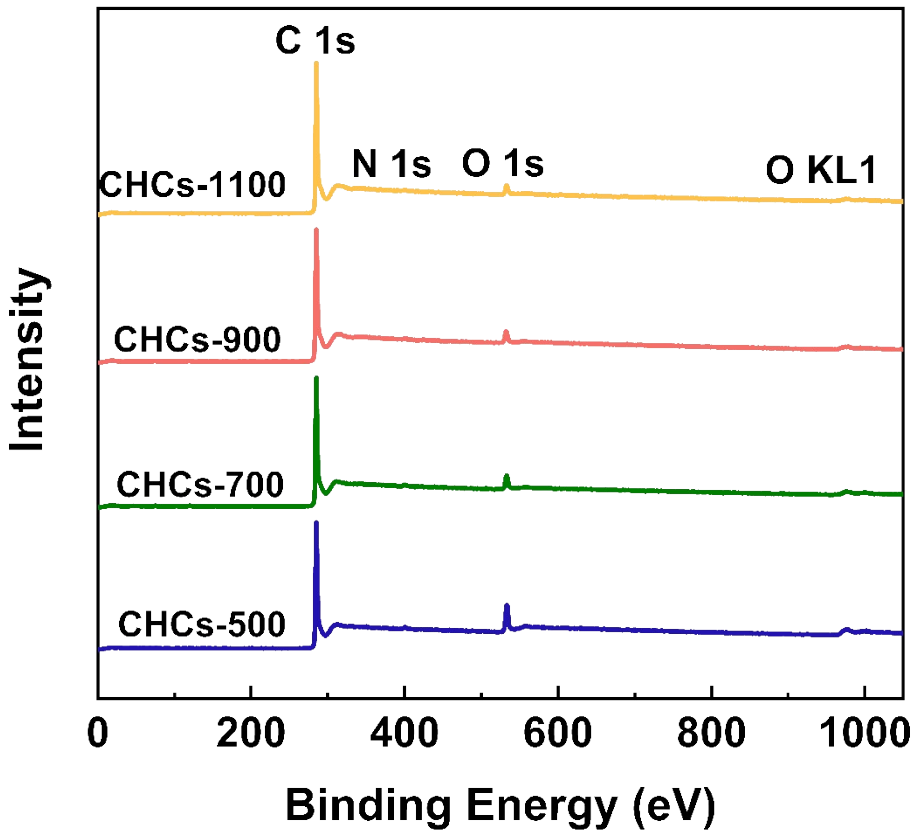

Fig. S3. XPS survey spectra of CHCs-T materials

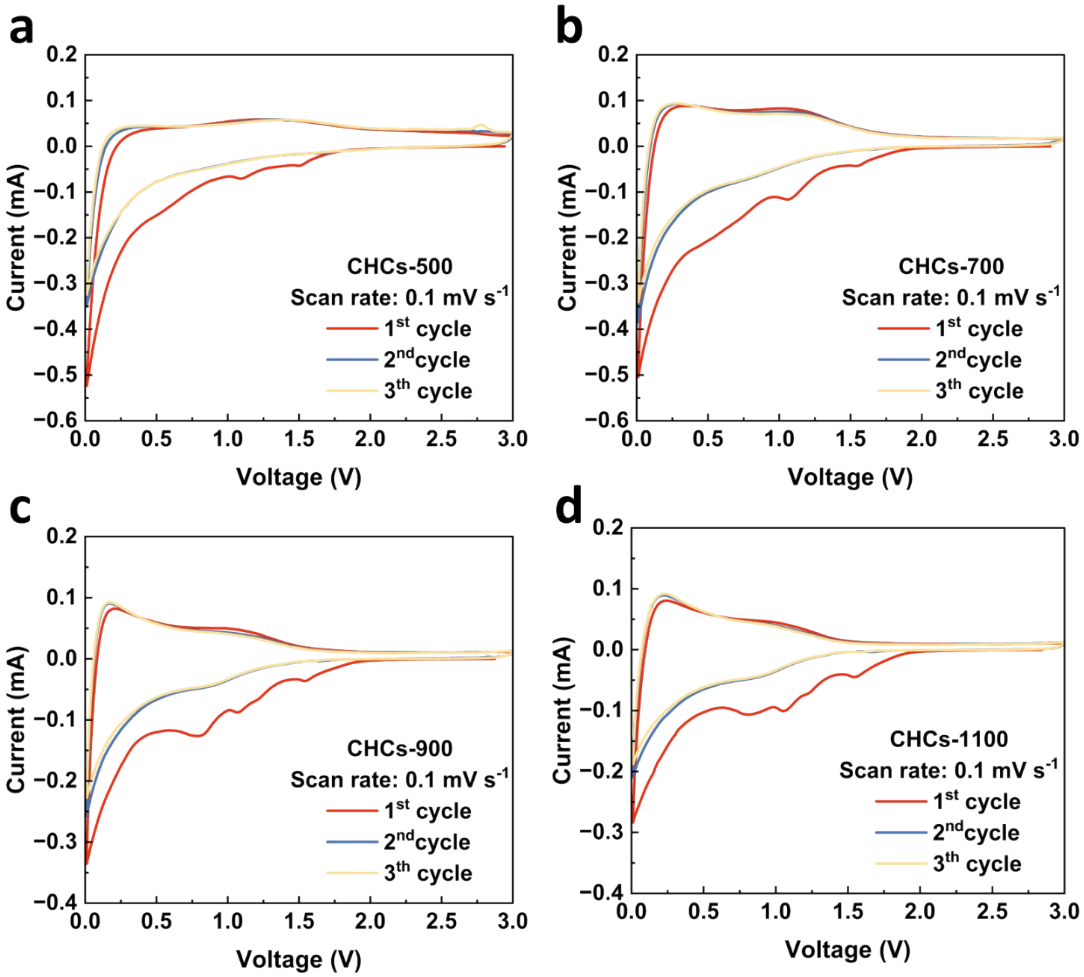

Fig. S4. The first, second, and third CV curves of the CHCs-T lithium-ion battery anodes: (a) CHCs-500; (b) CHCs-700; (c) CHCs-900; (d) CHCs-1100

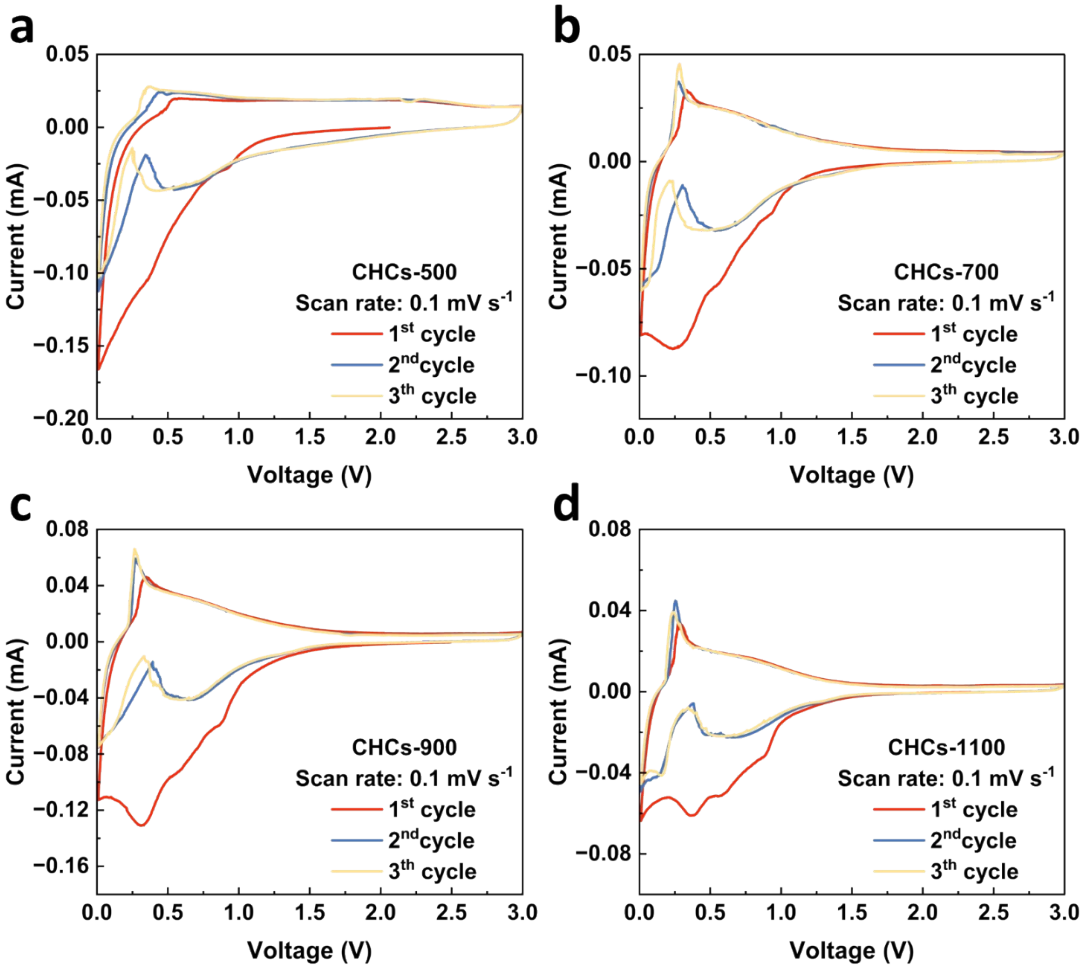

Fig. S5. The first, second, and third CV curves of the CHCs-T sodium-ion battery anodes: (a) CHCs-500; (b) CHCs-700; (c) CHCs-900; (d) CHCs-1100

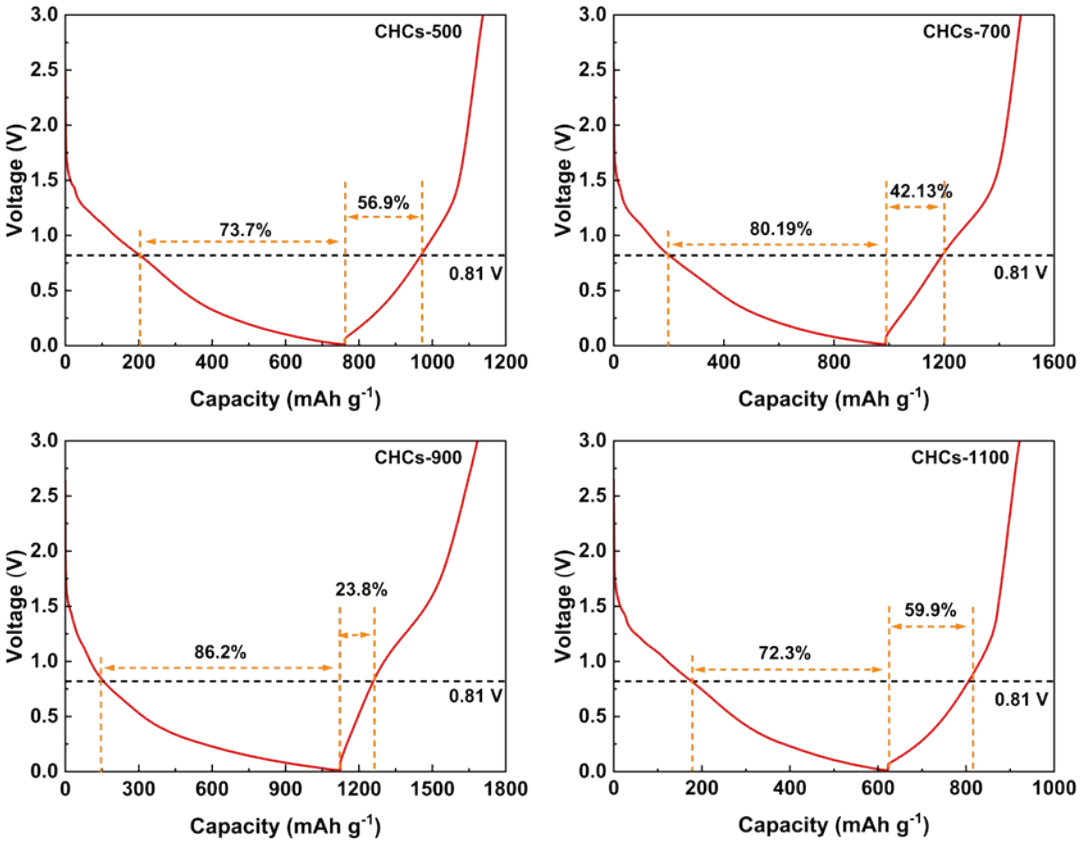

Fig. S6. Electrochemical voltage profile during the first lithiation/delithiation of the CHCs-T lithium-ion battery anodes: (a) CHCs-500; (b) CHCs-700; (c) CHCs-900; (d) CHCs-1100

.

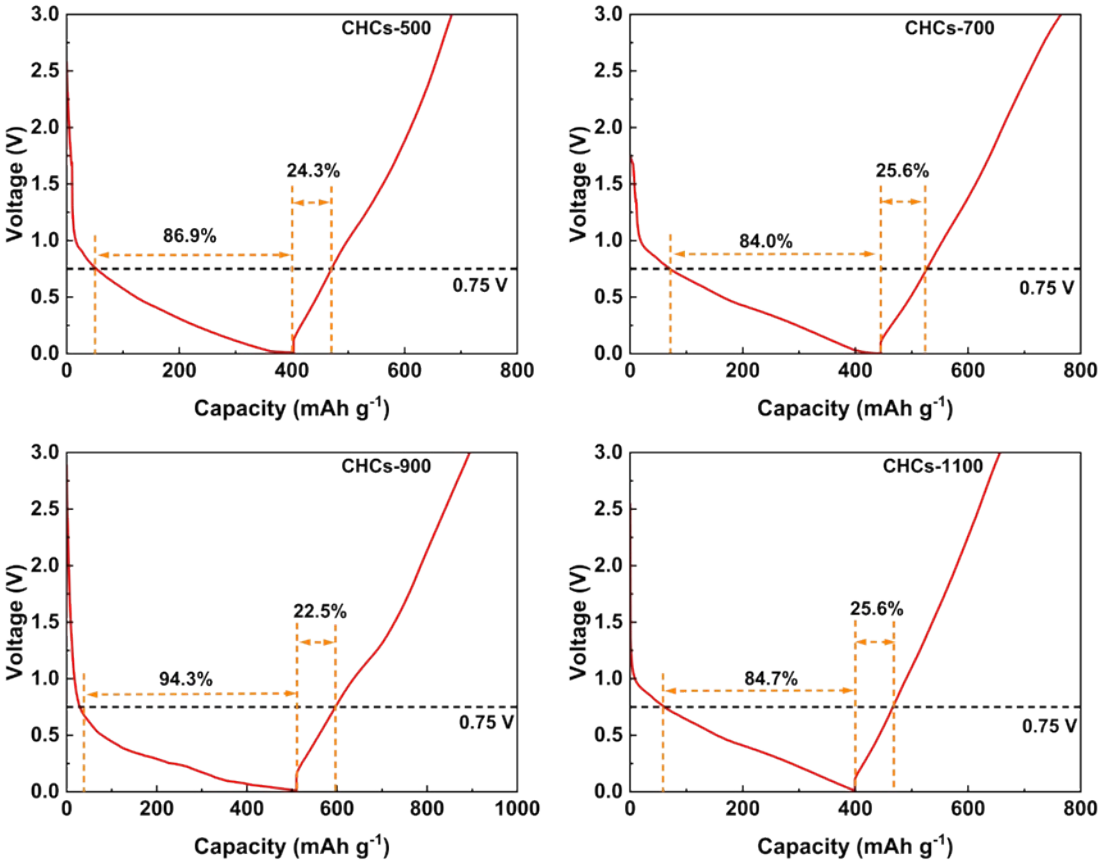

Fig. S7. Electrochemical voltage profile during the first lithiation/delithiation of the CHCs-T sodium-ion battery anodes: (a) CHCs-500; (b) CHCs-700; (c) CHCs-900; (d) CHCs-1100

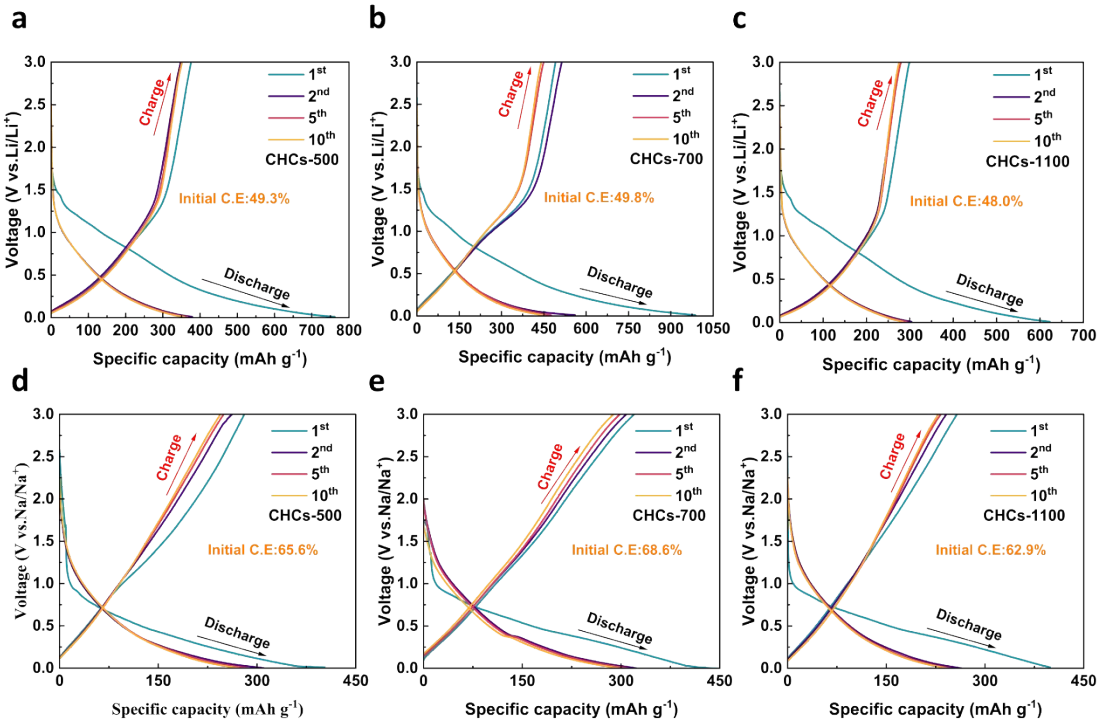

Fig. S8. Electrochemical lithium storage performance: (a-c) galvanostatic charge–discharge profiles at 200 mA g^{-1} of CHCs-500, CHCs-700, and CHCs-1100. Electrochemical sodium storage performance: (d-f) galvanostatic charge–discharge profiles at 200 mA g^{-1} of CHCs-500, CHCs-700, and CHCs-1100

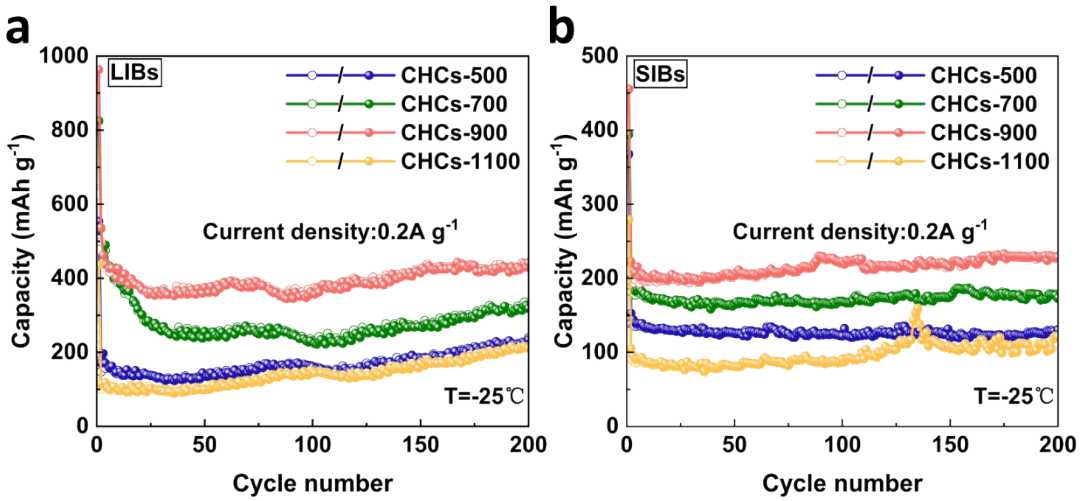

Fig. S9. Low temperature performances at -25℃: (a) cycling performance at 200 mA g^{-1} of CHCs-500, CHCs-700, CHCs-900, and CHCs-1100 for LIBs; (b) cycling performance at 200 mA g^{-1} of CHCs-500, CHCs-700, CHCs-900, and CHCs-1100 for SIBs

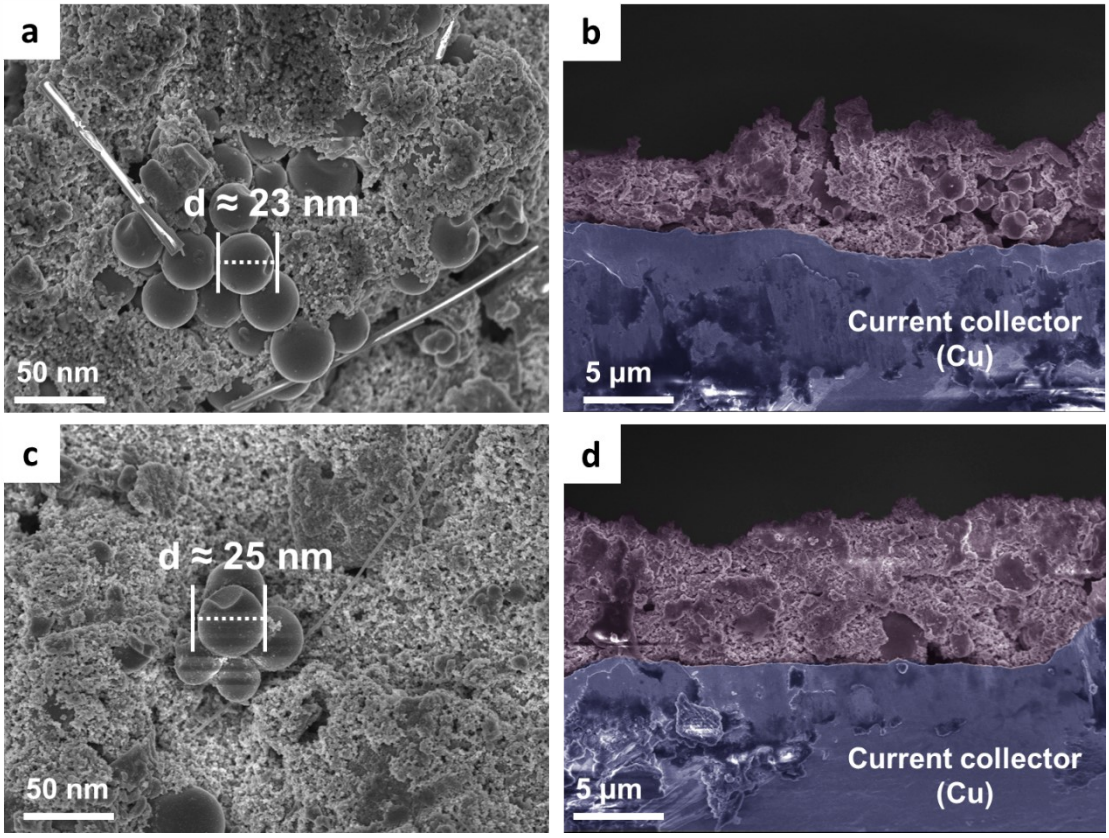

Fig. S10. FE-SEM images of the CHCs-900 anode: (a) Planes and (b) Cross-sections before cycling; (c) Planes and (d) Cross-sections after 1050 cycles at 1.0 A g^{-1}

Table S3. The comprehensive electrochemical performance of CHCs-900 anode with other carbon-based anodes for LIBs from the recent published literature

Ref.	Sample	First charge/discharge specific capacity	ICE	Rate performance	Cycle performance
		mAh g^{-1}	%	mAh g^{-1}	mAh g^{-1}
This work	CHCs-900	575.3/1123.5 at 0.2 A g^{-1}	51.2	217.8@10.0 A g^{-1}	352.2 (1.0 A g^{-1} for 1050 cycles)
45	LPG	250.0/600.0 at 0.1 A g^{-1}	41.7	225.0@0.5 A g^{-1}	225.0 (0.1 A g^{-1} for 100 cycles)
46	ANC	293.4/600.0 at 1.0 A g^{-1}	48.9	104.6@1.0 A g^{-1}	206.9 (1.0 A g^{-1} for 300 cycles)
47	HC-800	528.7/656.1 at 0.04 A g^{-1}	80.6	200.0@2.0 A g^{-1}	300.0 (0.5 A g^{-1} for 300 cycles)
48	CSC-2	402.5/872.1 at 0.1A g^{-1}	46.1	283.0@2.0 A g^{-1}	281.0 (0.5 A g^{-1} for 100 cycles)
49	BPW@H_3PO_4	307.0/942.0 at 0.05 A g^{-1}	32.6	131.0@5.0 A g^{-1}	272.0 (0.05 A g^{-1} for 100 cycles)
50	HC-1100	428.0/940.7 at 0.1A g^{-1}	45.5	165.0@3.0 A g^{-1}	265.0 (0.5 A g^{-1} for 500 cycles)

Table S4. The comprehensive electrochemical performance of CHCs-900 anode with other carbon-based anodes for SIBs from the recent published literature

Ref.	Sample	First charge/discharge specific capacity	ICE	Rate performance	Cycle performance
		mAh g^{-1}	%	mAh g^{-1}	mAh g^{-1}
This work	CHCs-900	369.6/509.5 at 0.2 A g^{-1}	72.5	141.5@10.0 A g^{-1}	271.9 (1.0 A g^{-1} for 1050 cycles)
51	BHC1100	217.8/371.0 at 0.05 A g^{-1}	58.7	—	150.0 (0.25 A g^{-1} for 100 cycles)
52	HC-C	294.0/463.0 at 0.05 A g^{-1}	63.0	—	270.0 (0.05 A g^{-1} for 100 cycles)
53	BPPG-1100-A	385.0/567.0 at 0.05 A g^{-1}	67.8	155.0@1.0 A g^{-1}	298.0 (0.05 A g^{-1} for 300 cycles)
54	IWC-1000	264.0/1196.0 at 0.1 A g^{-1}	22.1	278.0@1.0 A g^{-1}	176.0 (0.1 A g^{-1} for 1000 cycles)
55	CGDHC-CMC	113.6/335.5 at 0.05 A g^{-1}	34.0	—	118.6 (0.05 A g^{-1} for 100 cycles)
56	3DHSC-460	215.5/359.1 at 0.05 A g^{-1}	60.0	97.0@5.0 A g^{-1}	200.7 (0.05 A g^{-1} for 100 cycles)
57	HC-SC	241.0/261.0 at 0.05 A g^{-1}	92.7	122.0@1.0 A g^{-1}	241.0 (0.05 A g^{-1} for 60 cycles)
58	N-ZAHC	402.0/528.0 at 0.05 A g^{-1}	75.9	128.0@3.2 A g^{-1}	185.7 (0.4 A g^{-1} for 500 cycles)
59	EHC-Cell#2	241.0/487.0 at 0.05 A g^{-1}	49.5	43.0@1.0 A g^{-1}	150.0 (0.05 A g^{-1} for 300 cycles)
60	CDC-900	256.2/562.1 at 0.05 A g^{-1}	45.6	134@1.0 A g^{-}	188.0 (0.1 A g^{-1} for 200 cycles)

Table S5. The summary of quasi-spherical biochar fabrication

Ref.	Preparation method	Advantages	Disadvantages
61	Hard templating	● Maintain original form. ● Apply to a variety of materials and sizes. ● Facilitate scale-up.	◆ Morphological control is limited by the template. ◆ Causes environmental pollution.
62	Spray pyrolysis	● Easy operation of the process. ● Short processing time. ● Good particle reactivity.	◆ Uncontrolled pyrolysis processes ◆ Waste of large amounts of solvent ◆ Poor homogeneity of the material.
63	Ball milling	● Economical and environmentally friendly.	◆ Highly instrument dependent. ◆ Material particle size distribution is not uniform.
64	Chemical vapor deposition	● The reaction process is easy to control ● The reaction temperature is relatively low.	◆ Difficulty in realizing mass production. ◆ Poor cost-effectiveness and environmental benefits.
65	Hydrothermal carbonization	● Reaction conditions gentle. ● The chemical process is controllable. ● Low cost. ● Green and sustainable.	◆ Complex reaction process. ◆ Poor material conductivity.